Supporting Information

Roberts et al. 10.1073/pnas.1201872109

SI Methods

Site-Directed Mutagenesis and Expression. The QuikChange mutagenesis kit (Stratagene) was used to generate cysteine point mutations of residues Glu52-Gly96 using the human P2X1 receptor plasmid or the P2X1-2NβTM1 chimera (1) as the template, as described previously (2). All P2X1 mutants were verified by DNA sequencing (Automated ABI Sequencing Service, University of Leicester, United Kingdom).

WT and mutant receptors were transcribed to produce sense strand cRNA (mMessage mMachine; Ambion), as described previously (2). Manually defolliculated stage V *Xenopus laevis* oocytes were injected with 50 nL (50 ng) of cRNA using an inject + Matic microinjector (L. A. Gaby, Inject + Matic, Geneva, Switzerland) and stored at 17 °C in ND96 buffer (96 mM NaCl, 2 mM KCl, 1.8 mM $CaCl_2$, 1 mM $MgCl_2$, 5 mM sodium pyruvate, 5 mM Hepes, pH 7.6). Media was changed daily before biochemical analysis 3–5 d later.

Accessibility of Introduced Cysteine Residues. MTSEA-biotin (*N*-Biotinoylaminoethyl methanethiosulfonate) (Toronto Research Chemicals) was used to determine the accessibility of the various cysteine mutants. For WT and P2X1 receptor mutants, 10 oocytes injected with WT or mutant receptor cRNA were preincubated at room temperature for 30 min in 0.5 mL of ND96 solution containing either 15 U/mL apyrase (type III, A7646; Sigma) or ATP (1 mM). After the preincubation period, an additional 0.5 mL of ND96 was added containing either, 15 U/mL apyrase and 2 mM MTSEA-biotin, or 1 mM ATP and 2 mM MTSEA-biotin. Oocytes were incubated for an additional 30 min before MTSEA-biotinylation of the P2X1 receptor was assessed, as described previously (3). For biotinylation studies on the P2X1-2NβTM1 chimera background, oocytes were either preincubated with apyrase or ATP for 1 min before a further 5-min incubation with apyrase/MTSEA-biotin or ATP/MTSEA-biotin before MTSEA-biotinylation was assessed, as described previously (3). For mutants where biotinylation was detected, densitometry was used to determine whether ATP treatment had any effects.

Molecular Modeling. The trimeric assembly of the human P2X1 receptor (residues 33–352) was modeled in Modeler v9.7 (4) based on the zebrafish P2X4 structure (PDBid: 3I5D) as template. Target and template share 44% sequence identity and 67% sequence similarity based on a BLAST alignment. The best model was selected based on Modeler's scoring function and external validation via Whatcheck (5) and PROSA (6). NACCESS [Hubbard, S. J. and Thornton, J. M. (1993), Department of Biochemistry and Molecular Biology, University College London, United Kingdom, Computer Program, Department of Biochemistry and Molecular Biology, University College London] was used to determine the solvent accessibility of individual residues in the trimeric model. Residues with an absolute side chain accessibility >5 $Å^2$ were considered as accessible. All figures illustrating molecular modeling results were prepared in PyMOL (Molecular Graphics System, Version 1.2r3, Schrödinger), internal cavities were visualized using the Hollow tool (7).

P2X1 Receptor Purification. Human P2X1 receptor in pcDNA3 vector was tagged by the C-terminal addition of a $FLAGHis_6$ motif. The human P2X1 $FLAGHis_6$ plasmid was transfected into HEK293 cells and selected for stable expression. Human P2X1 $FLAGHis_6$ receptors were isolated using anti-FLAG M2 Affinity agarose gel/column. Starting material of 10 × 175-cm^2 flasks of HEK293 cells stably expressing human P2X1 $FLAGHis_6$ were lysed using buffer containing 150 mM NaCl, 40 mM Tris HCl (pH7.5), 8 mM Tris base, 1% n-Octyl glucoside, and protease inhibitor mixture (Sigma). Cell lysate was cleared by centrifugation (16,000 × *g* for 15 min) and supernatant rolled overnight with 4 mL of anti-FLAG M2 affinity agarose gel (Sigma). The agarose beads were placed in a column and flow-through collected. Beads were washed four times with lysis buffer and a sample collected at each wash stage. Proteins were eluted with 1 mL aliquots of 0.1 mg/mL 3× FLAG peptide followed by two 1-mL aliquots of 0.1 M Glycine pH3.5. Samples of fractions (10 μL) collected from each step were Western blotted with anti-P2X1 antibody (Alomone) at 1:1,000 dilution (as used previously) and positive fractions pooled and concentrated using Amicon Ultra 4 30,000 MWCO centrifugal filters (Millipore). A sample of purified $FLAGHis_6$-tagged human P2X1 receptor and BSA standards were analyzed on a 10% SDS PAGE gel and stained using InstantBlue (Expedeon). The stained P2X1 band was excised, trypsin digested, and checked using mass spectrometry. LC-MS/MS analysis was carried out using either 4000 Q-Trap system or Thermo Orbitrap (PNACL, University of Leicester, Leicester, United Kingdom). Postrun MS/MS ion searches were carried out on Mascot (Matrix Science). Purified $FLAGHis_6$-tagged human P2X1 receptor was snap-frozen in liquid nitrogen and stored at −80 °C.

Transmission Electron Microscopy and Single Particle Analysis. Purified P2X1 protein (50 μg/mL) was either adsorbed directly on to glow-discharged carbon-coated copper grids for 30 s (native) or incubated for 1 min in 1 mM ATP before adsorption (ATP-bound). Grids were washed twice with either 10 μL water (native) or 10 μL 1 mM ATP (ATP-bound) and negative-stained in 2% (wt/vol) uranyl acetate for 1 min. Grids were imaged in a Jeol JEM-1200 at 100 kV equipped with a Gatan Orius 2k camera. Images were recorded at either 3.30 or 5.16 Å/pixel. EMAN software (8) was used to manually select, filter, and process either 6,333 (native) or 4,370 (ATP-bound) particles in either 64 × 64 pixel (3.30 Å/pixel) or 42 × 42 pixel (5.16 Å/pixel) boxes. To minimize model bias, both structures were refined over 12 iterations using the same starting model, which was prepared from the native particle dataset using the "startcsym" command. C3 symmetry was applied throughout. Fourier shell correlation of structures prepared from even/odd particles using "eotest" indicated final resolutions of 22 Å (native) and 21 Å (ATP-bound) (Fig. S5). Structure-factor amplitudes were corrected using those derived from the zebrafish P2X4.1 crystal structure (PDB: 3I5D) and displayed at volume shells corresponding to at least three SD values above the mean density.

Electrophysiological Recordings. Two-electrode voltage-clamp recordings (at a holding potential of −60 mV) were carried out on cRNA injected oocytes using a GeneClamp 500B amplifier with a Digidata 1322 analog-to-digital converter and pClamp 8.2 acquisition software (Axon Instruments, Molecular Devices), as previously described (2). Native oocyte calcium-activated chloride currents in response to P2X receptor stimulation were reduced by replacing 1.8 mM CaCl2 with 1.8 mM BaCl2 in the ND96 bath solution. ATP (Mg salt) was applied via a U-tube perfusion system (Sigma). ATP was applied at 5-min intervals to evoke reproducible ATP responses. DTT (10 mM) was added to the perfusate.

1. Allsopp RC, Evans RJ (2011) The intracellular amino terminus plays a dominant role in desensitization of ATP-gated P2X receptor ion channels. *J Biol Chem* 286: 44691–44701.
2. Ennion S, Hagan S, Evans RJ (2000) The role of positively charged amino acids in ATP recognition by human P2X(1) receptors. *J Biol Chem* 275:29361–29367.
3. Roberts JA, Evans RJ (2007) Cysteine substitution mutants give structural insight and identify ATP binding and activation sites at P2X receptors. *J Neurosci* 27:4072–4082.
4. Martí-Renom MA, et al. (2000) Comparative protein structure modeling of genes and genomes. *Annu Rev Biophys Biomol Struct* 29:291–325.
5. Hooft RW, Vriend G, Sander C, Abola EE (1996) Errors in protein structures. *Nature* 381: 272.
6. Wiederstein M, Sippl MJ (2007) ProSA-web: Interactive web service for the recognition of errors in three-dimensional structures of proteins. *Nucleic Acids Res* 35(Web Server issue):W407–W410.
7. Ho BK, Gruswitz F (2008) HOLLOW: generating accurate representations of channel and interior surfaces in molecular structures. *BMC Struct Biol* 8:49.
8. Ludtke SJ, Baldwin PR, Chiu W (1999) EMAN: Semiautomated software for high-resolution single-particle reconstructions. *J Struct Biol* 128:82–97.

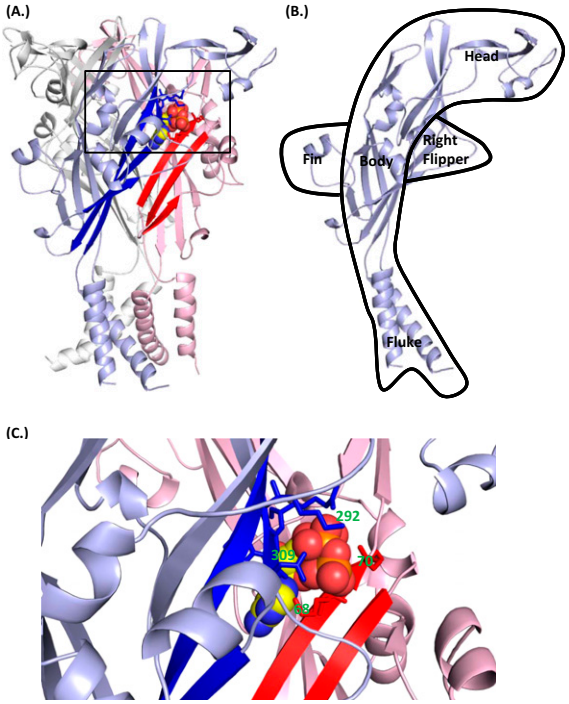

Fig. S1. (*A*) Homology model of the P2X1 receptor showing a cartoon representation of the three subunits in light blue, pink, and white. At one subunit interface residues contributing to the proposed ATP binding site are shown in blue from one subunit and red from the adjacent one. ATP is shown in spheres with the red/orange phosphate tail projecting out of the binding pocket. β-Sheet regions are shown in blue and red. (*B*) The blue subunit is shown with an overlay of a dolphin shape showing the cysteine-rich head region, the body, the right flipper, dorsal fin, and the transmembrane fluke. (*C*) Enlarged view of region identified by black box in *A*. Lysine residues 68 and 70 in the right-hand subunit are shown in red, lysine 309 and the NFR motif 290-292 are shown in blue, and the docked ATP molecule is shown in sphere representation.

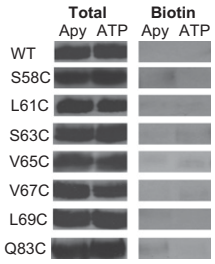

Fig. S2. P2X1 receptor mutants where MTSEA-biotinylation was not detected are expressed at normal levels. To determine the surface accessibility of the introduced cysteine residues, oocytes were incubated with MTSEA-biotin, biotinylated proteins isolated, separated by SDS-PAGE, and blotted with anti-P2X1 receptor antibody. Blots show MTSEA biotinylation was not detected from WT P2X1 and S58C, L61C, S63C, V65C, V67C, L69C, and Q83C receptors when pretreated with either apyrase (to break down endogenous nucleotides) or ATP (to activate the receptor). Total levels of WT and mutant P2X1 receptors are shown for the oocytes before isolation of biotinylated proteins and demonstrate that the lack of biotinylation does not result from reduced expression of the receptor, but to a lack of accessible cysteine residues on the WT or these mutant P2X1 receptors.

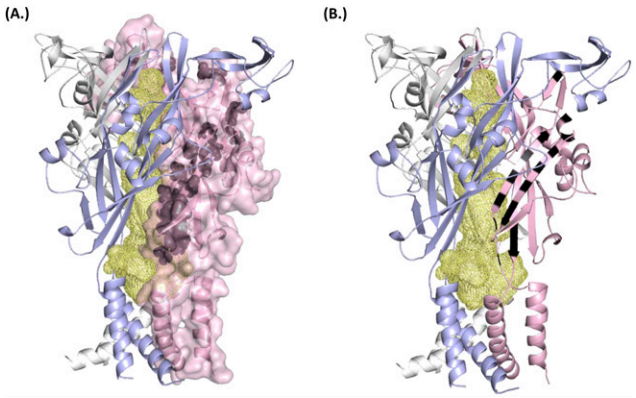

Fig. S3. (*A*) Homology model of the P2X1 receptor showing the three subunits in pink, light blue, and white; the central vestibules are shown as wheat mesh. The pink subunit is shown as a surface representation, the black spheres correspond to cysteine mutants that were not detected by MTSEA-biotinylation and are buried within the receptor. (*B*) Cartoon representation of the three subunits shows that the cysteine mutants that are inaccessible (black) are associated predominantly with alternate residues in two β-strands. The positions of the cysteine mutants face into one another consistent with these stands being closely packed to form a β-sheet.

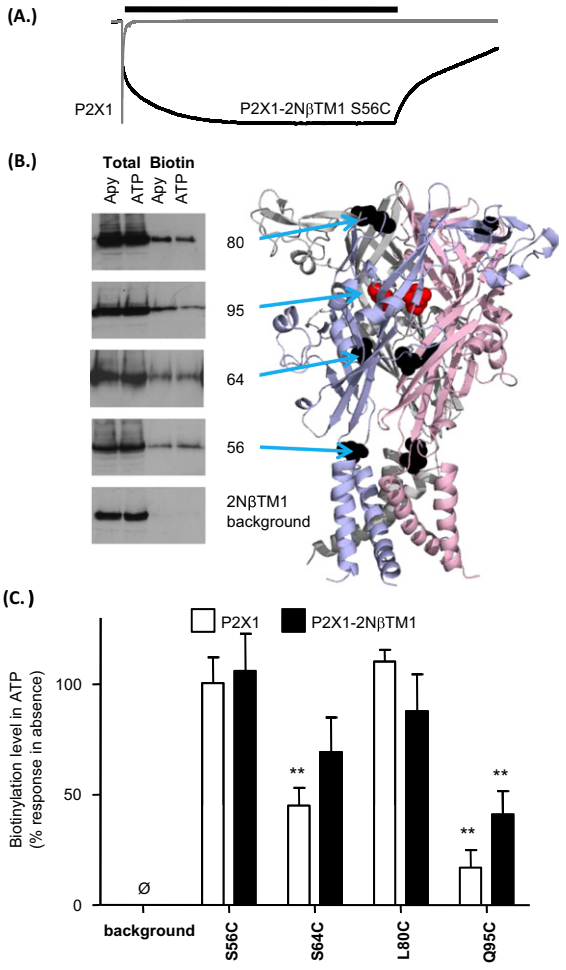

Fig. S4. (*A*) A 6-min ATP application (100 μM, period indicated by bar) evoked transient inward currents for the P2X1 receptor WT but currents showed little or no desensitization at P2X1-2NβTM1 cysteine mutants (peak current remaining at the end of a 360-s application 100 ± 0, 93.5 ± 3.3, 90.6 ± 2.9, 100 ± 0, and 99.3 ± 0.7% for P2X1-2NβTM1, and mutants S56C, S64C, L80C, and Q95C, respectively, $n = 3–7$). Figure shows normalized traces for P2X1 WT and P2X1-2NβTM1 S56C. (*B*) MTSEA-biotinylation on the P2X1-2NβTM1 background. (*Left*) Representative blots for the P2X1-2NβTM1 and cysteine mutants, showing total levels of receptor and MTSEA-biotinylated receptor in the absence (apyrase, Apy) or presence of ATP. (*Right*) A cartoon representation of the three subunits with the positions of the cysteine mutants as spheres, those with no change in biotinylation on ATP application in black, and ATP reduced biotinylation in red. (*C*) Densitometic analysis of any change in MTSEA-biotinylation at each point mutation following receptor activation with ATP on the P2X1 (data from Fig. 1, open columns) or P2X1-2NβTM1 receptor background (black columns). Inaccessibility of particular mutants to MTSEA biotin is indicated by Ø. Statistical analysis corresponds to whether ATP reduced the level of biotinylation for that particular mutant (**$P < 0.01$); results from at least five separate experiments from more than four batches of oocytes.

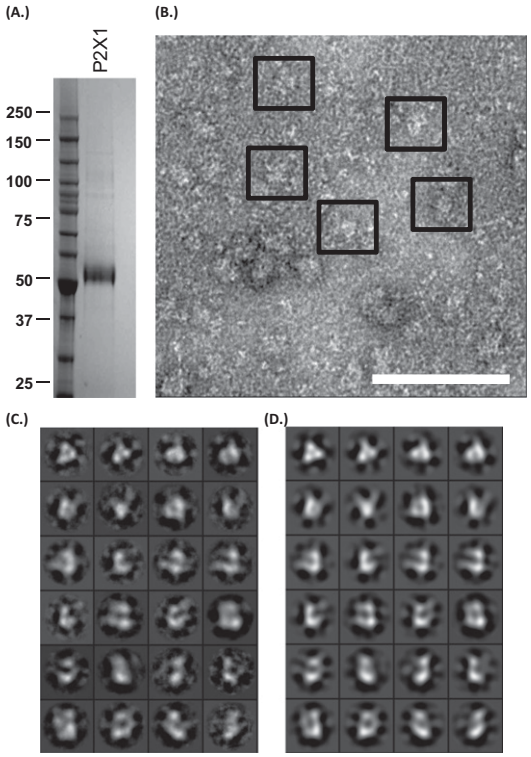

Fig. S5. (*A*) C-terminally HisFLag-tagged P2X1 receptors were purified; gel shows protein stain of molecular weight markers (*Left*) and purified P2X1 receptor (*Right*). The single band for P2X1 shows the purity of the sample; mass spectroscopy analysis also demonstrated no detectable contaminating proteins. Single-particle data. (*B*) Representative negatively stained transmission electron microscopy image field showing native P2X1 particles (indicated in 64 × 64-pixel boxes). (Scale bar, 50 nm.) (*C*) Selected 2D class averages used in structure refinement of the native dataset, showing top/bottom views through to side views (*Top Left* to *Bottom Right*). (*D*) Selected symmetrized reprojections from the final 3D structure. A good correlation between class averages and reprojections can be observed. Resolution measured at FSC = 0.5 was 22 Å for the native structure, and 21 Å for the ATP-bound structure.

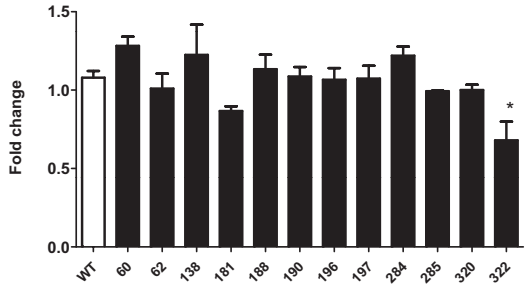

Fig. S6. To test whether the potentiating effects of DTT on double-cysteine mutants were not the result of an effect on the constituent single-cysteine mutants; the effects of DTT were determined on single-cysteine point mutations. Treatment with DTT had no effect on ATP-evoked currents, with the exception of 322C, where there was a small ~25% reduction in peak current amplitude. These results suggest that the potentiation in response to DTT seen for the double cysteine mutants resulted from an effect on an introduced disulphide bond. $*P < 0.05$.